Aalto-yliopisto
Aalto-universitetet
Aalto University

Master's Programme in Mechanical Engineering

Simulation of hydraulic damper using accumulator-based resonator

Martti Majander

Aalto-yliopisto
Aalto-universitetet
Aalto University

Author Martti Majander	
Title of thesis Simulation of hydraulic damper using accumulator-based resonator	
Programme Master's Programme in Mechanical Engineering	
Major Mechanical Engineering	
Thesis supervisor Prof. Jari Vepsäläinen	
Thesis advisor(s) D.Sc. (tech) Jyrki Kajaste	
Collaborative partner Valmet Technologies Oy	

Date 28.03.2025   **Number of pages** 44   **Language** English

Abstract

Vibration causes problems in industry, such as wear of components and manufacturing faults. Vibration may be caused by the centrifugal force generated by the rotation of an imbalanced part, for instance. As the frequency of the force causing the vibration is bear the natural frequency of the system, resonance occurs. Resonance must be avoided, as the amplified vibration may lead to catastrophic failure of the machinery.

Many applications have been developed to attenuate vibration. In this thesis a hydraulic damping system using a resonator with multiple pressure accumulators at various fluid line lengths was studied. The system damps vibration at a specific frequency in a similar manner to a double spring mass system, where maximizing pressure oscillation in turn increases the force required to continue vibration of the piston. Switching between different accumulators allows for multiple frequency curves of optimal system stiffness. This enables better damping as the system stiffness changes due to the force oscillation frequency changing or the cylinder being extended or retracted during operation. It also allows shifting the natural frequency of the system to at the very least avoid resonance.

In this thesis a simulation model of the system was made using MATLAB. The system was simulated and an experimental test setup using a single pressure accumulator was built based on the simulated results. Experimental measurements were processed and compared to the simulation results.

The simulated results matched the measured results well in terms of prediction of the optimal frequency, but the measured maximum stiffness was considerably lower than expected. The simulation result could be adjusted by increasing the viscosity, which was believed to be higher than expected due to coiled pipes used in the test setup. However, further research with more detailed models is recommended.

Keywords damping, vibration, pressure accumulator, hydraulic cylinder, stiffness, simulation

Tiivistelmä

Teollisuudessa tärinä aiheuttaa useita ongelmia, kuten osien kulumista ja viallisia tuotteita. Kun tärinää aiheuttavan voiman, kuten epätasapainossa olevan osan pyörimisen epäkeskeisyysvoiman, taajuus on lähellä järjestelmän ominaistaajuutta, ilmaantuu resonanssia. Resonanssia tulee välttää, sillä vahvistunut tärinä voi johtaa koneiston katastrofaaliseen pettämiseen.

Useita sovelluksia on kehitetty tärinän vaimentamiseen. Tässä diplomityössä tutkitaan hydraulista tärinänvaimenninta, jossa on useaa eri putkipituuksille asetettua paineakkua käyttävä resonaattori. Järjestelmä vaimentaa tärinää tietyllä taajuudella kaksinkertaisen jousi-massasysteemin kaltaisesti, ja painevärähtelyn maksimointi kasvattaa voimaa, jota vaaditaan männän värähtelyliikkeen jatkamiseksi. Vaihtelemalla kytkettynä olevia paineakkuja mahdollistettiin erilaisia taajuuskäyriä optimaaliselle järjestelmän jäykkyydelle, joka mahdollistaa parempaa vaimennusta systeemin ominaisuuksien muuttuessa, kuten herätevoiman värähtelytaajuuden muuttuessa tai sylinterin mäntää liikuttaessa. Se myös mahdollistaa järjestelmän ominaistaajuuden siirtämisen, jolloin voidaan vähintäänkin välttää resonanssia.

Tässä diplomityössä kehitettiin simulaatiomalli järjestelmästä MATLAB-ohjelmistoa käyttäen. Järjestelmää simuloitiin ja testilaitteisto yhdellä paineakulla rakennettiin simulaation tuloksiin perustuen. Mittaustulokset käsiteltiin ja niitä verrattiin simulaation tuloksiin.

Simulaatiot vastasivat mitattuja tuloksia hyvin optimaalisen taajuuden arvioinnissa, mutta mitattu maksimijäykkyys oli huomattavasti odotettua matalampi. Simulaatiotuloksia pystyttiin sovittamaan nostamalla viskositeettia, jonka uskottiin olevan odotettua suurempi testijärjestelmän kierreputkien takia. Tulevaisuudessa järjestelmän tutkiminen yksityiskohtaisemmalla mallilla olisi suositeltavaa.

Avainsanat vaimennus, tärinä, paineakku, hydraulisylinteri, jäykkyys, simulointi

Contents

Symbols and abbreviations

Symbols

A	[m²]	Area
A_{th}	[m²]	Accumulator throat cross-sectional area
B	[Pa]	Bulk modulus
B_0	[Pa]	Nominal bulk modulus
B_1	[Pa]	Effective bulk modulus
C_{acc}	[m⁴s²/kg]	Accumulator capacitance
C_{hydr}	[m⁴s²/kg]	Hydraulic capacitance
c	[-]	Damping coefficient
c_m	[-]	Accumulator damping coefficient
c_s	[m/s]	Speed of sound
D	[m]	Diameter
D_h	[m]	Hose diameter
D_p	[m]	Pipe diameter
E	[Pa]	Young's modulus
F	[N]	Force
F_a	[N]	Force oscillation amplitude
f	[Hz]	Frequency
I	[A]	Electric current
i	[-]	Index
K	[N/m]	Hydraulic cylinder stiffness
K_o	[N/m]	Hydraulic fluid stiffness
K_r	[N/m]	Piston rod axial stiffness
K_c	[N/m]	Cylinder barrel expansion stiffness
K_p	[N/m]	Metal pipe expansion stiffness
K_h	[N/m]	Hose expansion stiffness
K_s	[N/m]	Sealing ring deformation stiffness
k	[N/m]	Stiffness (spring constant)
k_{dyn}	[N/m]	Dynamic stiffness
L	[H]	Inductance
L_{hydr}	[kg/m⁴]	Hydraulic inductance
l_{th}	[m]	Accumulator throat length
l	[m]	Length of pipe
l_{T-pipe}	[m]	Length of T-pipe
P	[Pa]	Pressure
P_{acc}	[Pa]	Accumulator inlet pressure
Q	[m³/s]	Volumetric flow rate
R	[Ω]	Electrical resistance

R_{hydr}	[kg/m⁴s]	Hydraulic resistance
U	[V]	Voltage
V	[m³]	Volume
v	[m/s]	Flow velocity
x	[m]	Displacement
x_a	[m]	Vibration amplitude
α	[-]	Ratio of air volume to fluid
λ	[m]	Wavelength
μ	[kg/ms]	Dynamic viscosity
ν	[m²/s]	Kinematic viscosity
ρ	[kg/m³]	Density
τ	[Pa]	Shear stress
ω	[rad/s]	Angular velocity
ω_{acc}	[rad/s]	Accumulator specific angular velocity

Abbreviations

ECA	Expansion Chamber Attenuator
FFT	Fast Fourier Transform
PQ	Pressure-Flow Rate

1 Introduction

Vibration is a phenomenon that occurs in nearly all industrial machines. It is caused by reciprocating or other repetitive movements, such as the rotary motion of a part with mass imbalance. Vibration causes many issues, some of which are wear of machine components, noise, or inaccuracies in the control of the system. In a paper winder (Figure 1), drum vibrations and other dynamical phenomena limit the speed of the winding process (Jorkama 1996). Vibrations at a frequency near the system's natural frequency are greatly amplified, which may lead to a catastrophic failure of the machine. (Randall 2021)
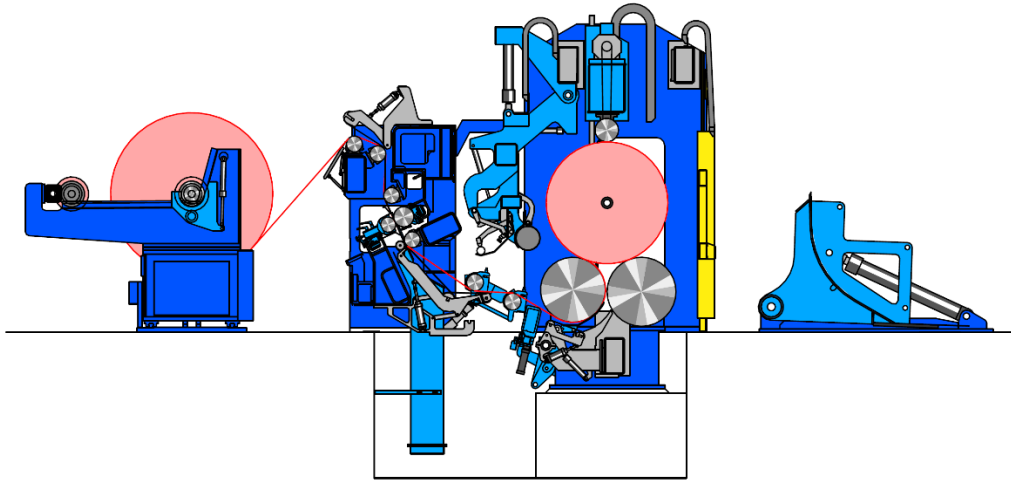

Figure 1. A two-drum paper winder. (Jorkama 1996)

In hydraulic applications, pressure oscillation causes similar issues, also including leakage. Many components have been developed for damping pressure oscillation. As reflective dampers change the system's dynamic response, they may also be used to amplify pressure oscillation in the fluid in response to vibration and therefore increase the system's mechanical stiffness. As a simplified example, a double spring-mass system may be compared to this, with the hydraulic fluid oscillating instead of, for instance, the piston of a hydraulic cylinder. (Ijas 2007)

As paper winders wind customer rolls, the piston of hydraulic cylinder used as a damper moves as the roll diameter increases. The resulting change in chamber volume changes the dynamic response of the damper during operation of the machine. This in turn could allow the damper's frequency for optimal stiffness to follow the rotation frequency of the paper roll, since it is decreased over the process to limit the velocity of the paper surface. (Närvänen 2024)

This study focuses on a digitally adjustable hydraulic damper which could be used to damp oscillations in applications such as a paper winder. In the

thesis, a MATLAB Simulink model is created to simulate the frequency response and determine stiffness. Based on the simulations, a test set up is built. Testing is performed and the measured results are compared to the simulations.

1.1 Aim of the study

The aims of this study are:
- Development of a simulation model of the hydraulic cylinder damping system based on literature in the field of hydraulics.
- Conducting simulations to find the optimal parameters for the vibration damper system at a desired frequency range.
- Construction of an experimental test system based on simulations.
- Comparison of the performance of the simulation model against experimental test results.

The main research question is: How well can be frequency of optimal stiffness be simulated and what is relevant to the simulation accuracy of the frequency?

1.2 Structure of the study

This study consists of seven chapters. The introduction chapter, in which the problem and study is briefly introduced, is followed by a background section relevant theory and components are discussed. Chapter 3 is the literature review which covers previous studies related to the problem and topic. Chapter 4 covers the methodology of modelling and the measurements. In chapter 5 results are displayed. A discussion chapter follows in which the effectiveness of chosen methods. The relevance and accuracy of the results are also discussed. Finally, there is a conclusion chapter where the study and its findings are summarised.

2 Background

This chapter explains the phenomena relevant to the problem. First, stiffness is explained, after which a hydraulic cylinder is discussed. Following a brief introduction to hydraulic fluid properties, the approximation of the dynamics of a fluid power system and its components are explained.

2.1 Stiffness

Stiffness is a property describing the resisting force that results from a change in length to a body. Static stiffness k is measured under a static load, and is defined as

$$k = \frac{\Delta F}{\Delta x} \tag{1}$$

where ΔF is the force and Δx is the corresponding deflection. Dynamic stiffness is measured under periodic loads, which are often seen in rotating machinery. Vibration is the resulting periodic motion caused by such loads. Dynamic stiffness k_{dyn} is defined similarly to static stiffness, as

$$k_{dyn} = \frac{F_a}{x_a} \tag{2}$$

where F_a is the amplitude of the periodic load and x_a is the amplitude of the corresponding vibration. The phase shift between the force and the displacement is also important (Mobley 1999). In a hydraulic cylinder system, multiple factors and components affect the stiffness (Feng, et al. 2017).

2.2 Hydraulic Cylinder

Hydraulic cylinders are linear actuators that are operated by force differences caused by pressure in cylinder chambers. Double acting cylinders, which include two chambers for pressure formation, are most used. A differential hydraulic cylinder and its components can be seen in Figure 2. The parts numbered are the cylinder (1), hydraulic oil or a cylinder chamber (2), piston sealing (3), rod sealing (4), rod (5), hoses (6), pipes (7).

In a symmetrical cylinder, the cylinder rod extends through both chambers. A differential cylinder only has a rod on one side of the piston. Due to the resulting difference in piston surface area for each chamber, flow into a chamber is different than the flow out of the other when the piston moves at constant speed. Similarly, force balance requires a higher pressure on the side without the rod compared to the rod chamber. (Mobley 2000)
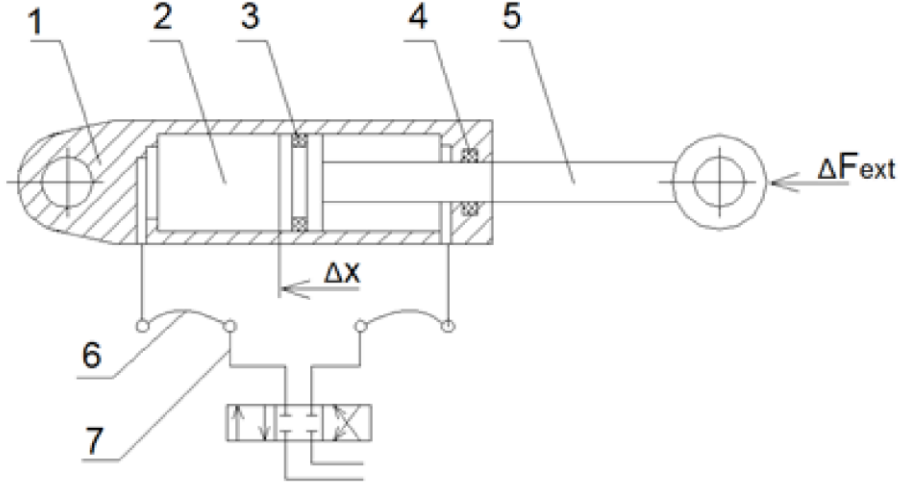
Figure 2. Hydraulic cylinder. (Feng, et al. 2017)

Feng et al. (2019) presents a stiffness model for a hydraulic cylinder. The average accuracy of their model showed an over 15 % improvement over stiffness models presented in literature at the time. The model they present is

$$\frac{1}{K} = \frac{1}{K_o} + \frac{1}{K_r} + \frac{1}{K_c} + \frac{1}{K_p} + \frac{1}{K_h} + \frac{1}{K_s} \tag{3}$$

where K is the hydraulic cylinder stiffness, K_o is the stiffness of the hydraulic fluid, K_r is the piston rod axial stiffness, K_c is the cylinder barrel expansion stiffness, K_p is the metal pipe expansion stiffness, K_h is the expansion stiffness of hoses and K_s is the deformation stiffness of sealing rings. The model doesn't account for stick slip.

A phenomenon known as stick-slip may affect hydraulic cylinders, operated at low speeds, where switching between static and dynamic friction causes abrupt jerks and stops instead of constant and continuous movement. Friction in the cylinder is caused by contacts between seals and cylinder surfaces, in which elastic deformation may also occur before movement. (Owen 2001)

The mathematical model presented in equation 3, also used in the thesis of Lu (2021), was modified in the thesis of Sirviö (2023) to suit a four-chamber hydraulic cylinder. A four-chamber hydraulic cylinder has four chambers that can be pressurised (Figure 3).
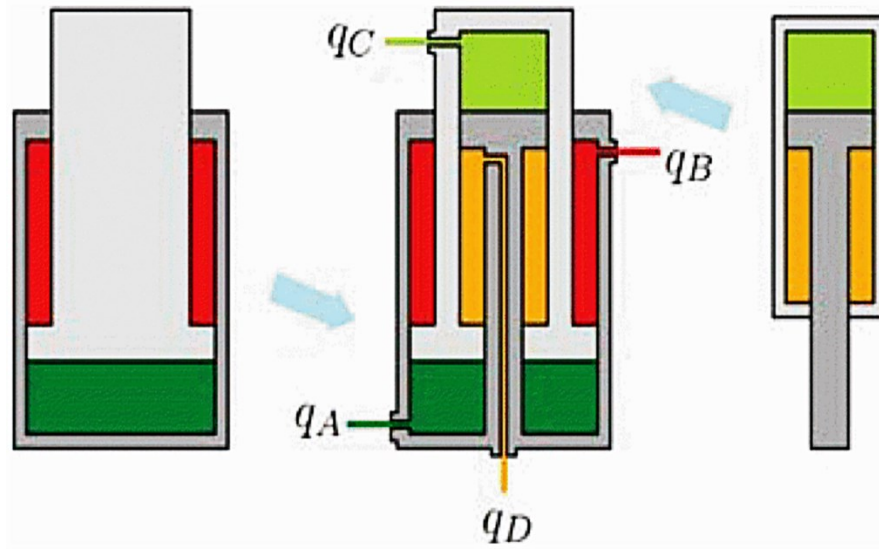
11

Figure 3. Drawing of a four-chamber hydraulic cylinder, and two differential cylinders it can be considered as. Modified from (Xiao-Ming, Luo and Xin 2016)

Two of the chambers can be pressurised to retract the cylinder piston and two of them extend it. A four-chamber cylinder can be used with two different fluids, and it could be operated with two separate systems or configurations. Due to increased total piston surface area, four-chamber cylinders are stiffer than traditional cylinders. A disadvantage is that their structure is more complex, leading to increased manufacturing costs, for instance. A four-chamber hydraulic cylinder is not used in this study, as they're less commonly used, and the advantages they offer are not considered necessary in this study.

2.3 Hydraulic Fluid Properties

The main objectives of hydraulic fluids are power transmission, lubrication, heat transfer and corrosion protection. Mineral oils are the most used in hydraulic applications due to suitable properties such as viscosity and stiffness, and relatively low cost. (Watton 2009)

Viscosity is a measure of a fluid's resistance to flow due to internal friction (Song 2018). Dynamic viscosity μ is defined by the Newtonian shear-stress equation:

$$\tau = \mu \frac{dv}{dy} \tag{4}$$

Where τ is the shear stress and dv/dy is the velocity transient of the flow (Watton 2009). From Poiseuille's equation, kinematic viscosity in a flow channel with a round cross-section is defined as:

$$\eta = \frac{p\pi r 4 t}{8Vl} \tag{5}$$

Where p is the pressure on the fluid, t is the time for volume V of the fluid to flow through the flow channel with a cross-sectional radius r and length l. (Kinkler 2011)

A fluid's bulk modulus measures the fluid stiffness and is a significant factor in the stiffness of a hydraulic system. The formula for bulk modulus B is

$$B = -V\left(\frac{\delta p}{\delta V}\right) \tag{6}$$

where V is the initial volume of the fluid, δp is the change in pressure and δV is the corresponding change in volume. (Kim and Murrenhoff 2012) The fluid bulk modulus of the hydraulic fluid varies due to multiple factors, such as air content, pressure, and temperature. The measurement and estimation of the effective bulk modulus in real systems is challenging (Yang, Feng and Gong 2011). A formula for effective bulk modulus is presented as

$$\frac{B_e}{B_0} = \frac{\left(\frac{p}{p_0}\right)^n + \alpha}{\left(\frac{p}{p_0}\right)^n + \frac{\alpha B_0}{np}} \tag{7}$$

where B_e is the effective bulk modulus, B_0 is the nominal bulk modulus of the fluid, p is the working pressure, p_0 is the atmospheric pressure, α is the ratio of the volume of air to the volume of fluid. For isothermal conditions, $n = 1$. The density of a fluid is defined as the ratio of mass to volume. For mineral oil, density increases as pressure increases and decreases as temperature increases. (Watton 2009)

2.4 Fluid Line Dynamics

The dynamics of the fluid in pipes and hoses are an important factor in determining the response of the system. In addition to friction losses, and added fluid compressibility, the compressibility of fluid lines cause inertia as pressure waves travel in the fluid. Curved fluid lines such as helical spiral pipes produce a frictional pressure loss increased by a secondary flow, which is caused by the centrifugal force acting on the fluid (Sun, et al. 2022).

Pressure peaks occur when a column of fluid flowing in a line stops when a valve closes, or a hydraulic actuator is stopped suddenly (Ijas 2007). Pressure transients also occur when a valve is opened quickly, and there is a difference in pressure between the two sides of the valve, such as in cases where a pressure accumulator is used as a pressure source with a valve for quick operation of a hydraulic cylinder. The magnitude of the pressure surge is affected by the air content of the fluid, the opening time of the valve, and the hydraulic resistance of the accumulator inlet. (Ichiryu 1973)

2.4.1 Electrical Analogy

In the electrical analogy, the pressure P and flow rate Q are compared to voltage U and current I, respectively. Thus, analogies to the fluid are given by resistance R, inductance I and capacitance C.

Hydraulic resistance R_{hydr} is derived from the equation of pressure loss in laminar pipe flow due to friction:

$$\Delta p = \frac{128 v \rho l}{\pi D^4} Q \tag{8}$$

where v is the kinematic viscosity of the fluid, ρ is the density of the fluid, l is the length of the fluid line and D is the hydraulic diameter, which is the internal diameter of the pipe in the case of a pipe with a circular cross-section. From this equation, as

$$\Delta U = RI \tag{9}$$

hydraulic resistance may be defined as

$$R_{hydr} = \frac{128 v \rho l}{\pi D^4} \tag{10}$$

Next, fluid compressibility is defined as

$$\Delta Q = \frac{V}{B} \frac{dP}{dt} \tag{11}$$

Where V is the nominal volume of the fluid and B is the fluid bulk modulus. As

$$\Delta I = C \frac{dU}{dt} \tag{12}$$

The hydraulic capacitance of a volume of fluid is derived as

$$C_{hydr} = \frac{V}{B} \tag{13}$$

Hydraulic inductance, or fluid inertia, is derived from the pressure drop due to fluid acceleration:

$$\Delta p A = \rho l A \frac{dv}{dt} \tag{14}$$

$$\Delta p = \frac{\rho l}{A} \frac{dQ}{dt} \tag{15}$$

Where U_{hydr} is the flow velocity and A is pipe cross-sectional area. Then, since

$$\Delta U = L \frac{dI}{dt} \tag{16}$$

Hydraulic inductance is defined from equation x as

$$L_{hydr} = \frac{\rho l}{A} \tag{17}$$

The electrical analogy may be used to simulate the effects of pipe friction, while accounting for fluid compressibility and the inertia it causes. The fluid line may also be considered as segments of fluid line connected in series, for lumped approximation. (Watton 2009)

2.4.2 Modal Approximation

The modal method is one of the most accurate, convenient and numerically stable method of approximating partial derivative equations used to model long pipes and hoses. Mäkinen et al. (2009) derived the method, showing transfer functions and state-space representations for modal approximation.

For the PQ (pressure-flow rate) model, which uses the flow rate at one end (flow into the pipe being positive) and pressure at the other end as inputs, the transfer functions are the following:

$$p_i = -\left(\frac{2}{(2i-1)\pi} P_0 + (-1)^i \frac{Z_0}{s} Q_1 \right) 2 w_i \left(\frac{s^2 + b_i \epsilon s}{s + \epsilon_i s + \omega_i^2} \right) \tag{18}$$

15

$$P_1 = P_0 + \sum_{i=1}^{n} (-1)^{i+1} p_i \qquad (19)$$

$$Q_0 \approx \frac{1}{Z_0(s + b_2\epsilon)} \sum_{i=1}^{n} \frac{(2i-1)\pi}{2} p_i \qquad (20)$$

$$\alpha_i = \frac{(2i-1)\pi}{2} \qquad (21)$$

$$\beta_i = \frac{(2i-1)\pi}{2n+1} \qquad (22)$$

$$b_1 = \left(2\sum_{i=1}^{n} \frac{w_i}{\omega_i^2} \right)^{-1} \qquad (23)$$

$$b_2 = \pi b_1 \sum_{i=1}^{n} (-1)^{i+1}(2i-1)\frac{w_i}{\omega_i^2} \qquad (24)$$

w_i is the window function component, P_0 and P_1 are the pressures at the ends of the line, Q_0 and Q_1 are the flow into the line ends, ω_i is the modal natural frequency coefficient and Z_0 is the line impedance. State space representation can be used. (Mäkinen, Piché and Ellman 2000)

2.5 Pressure Damping Methods

As vibration causes problems, such as noise and reliability issues, and as it may damage components, many methods of vibration damping have been developed. In this chapter, some of the common pressure vibration attenuators for hydraulic systems will be presented.

Vibration dampers are split into three types: Reflection or interference dampers, absorption dampers and active dampers. Of these, absorption dampers are considered unsuitable for lower frequencies, and active dampers are expensive. (Ijas 2007)

Reflection type dampers are additionally split into divergent type dampers and serial dampers. Divergent dampers are connected to the system in such a way that they branch out of the systems main fluid line, while serial dampers allow fluid flow through themselves, and are connected as a part of the fluid lines of system. (Ijas 2007)

Examples of divergent type resonators include the Helmholtz resonator and the T-pipe (Figure 4). They're similar in function in that they attenuate vibration with destructive interference at a relatively narrow frequency

range. Pressure waves of the tuned frequency are reflected in the opposite phase, causing vibrations at that frequency to become attenuated effectively.
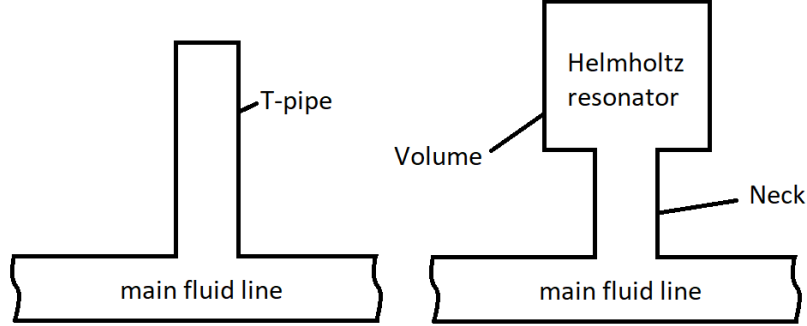

Figure 4. Illustration of a T-pipe (left) and Helmholtz resonator (right). Resonator volume shape varies.

The T-pipe is a dead-end branch of the main fluid line. The required length for a T-pipe in pressure pulsation attenuation of a certain frequency can be calculated with the following formula:

$$l_{T-pipe} = \frac{\lambda}{4} \tag{25}$$

Where λ is the wavelength

$$\lambda = \frac{c_s}{f} \tag{26}$$

Where c_s is the speed of sound in the fluid and f is the frequency of the pulsation. (Kela 2010)

For low frequencies, a T-pipe's length becomes impractical. T-pipes also have a much narrower attenuation band compared to the Helmholtz resonator, although it becomes wider with a larger pipe diameter. Another method of increasing the attenuation band is to use multiple T-pipes of varying lengths in a system. The Helmholtz resonator consists of a fluid volume and a pipe leading to the volume, called the neck of the resonator. It is more practical to implement and often has a wider attenuation band. (Ijas 2007)

An expansion chamber attenuator (ECA) is a serial damper that functions in a similar manner (Ijas 2007). ECAs are passages in the fluid line with a larger cross-sectional area than the rest of the pipes (Figure 5).
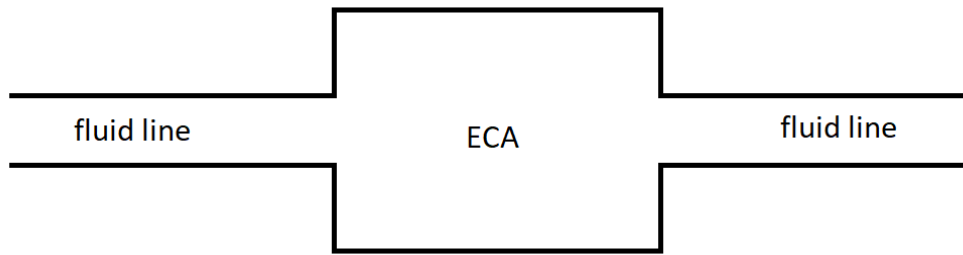
Figure 5. Illustration of an expansion chamber attenuator.

At the ECA entrance, the fluid volume increases suddenly. Pressure waves are reflected at the end of the attenuator and reflected again as they return. As a result, the reflection pressure waves damp vibration at the desired frequency by destructive interference. (Ortwig 2005)

2.5.1 Pressure Accumulators

A reflection type damper, a pressure accumulator has the disadvantage of wear to the elastic membrane or bladder, and a relatively expensive cost compared to the previously discussed, more simplistic resonators. Pressure accumulators are likely the most used damper type (Ijas 2007). They consist of a metal casing with an internal elastic bladder, such as illustrated in Figure 6, or a membrane. Another common type of accumulator is a piston accumulator, that houses a piston much like a hydraulic cylinder. The elastic component or piston separates a pressurised gas from the area where fluid may flow through an inlet. The gas, commonly nitrogen, accumulates energy as it is compressed when the hydraulic pressure causes oil flows in.
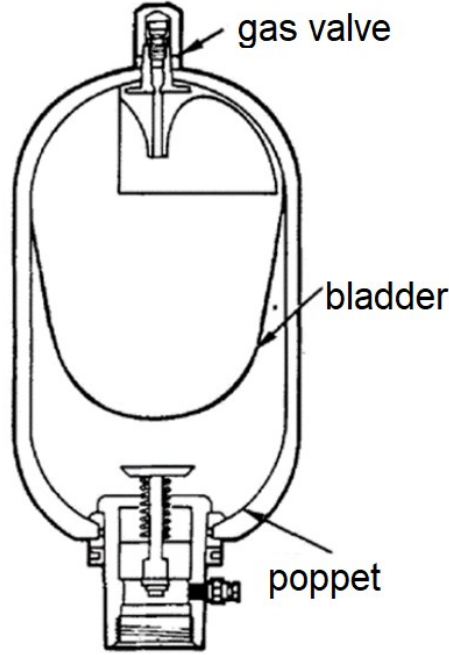
Figure 6. Bladder Accumulator with some parts indicated. A poppet prevents the bladder, which separates the fluid and the gas, from entering the accumulator neck. Modified from: (Mobley 2000)

Part of the stored energy in accumulators is converted to heat energy as the gas compresses and expands. Ortwig categorises accumulators as absorber type-silencers due to this (Ortwig 2005). However, Ijas categorises them as reflecting, likely due to the spring-like characteristic of the gas compressibility. Pressure accumulators are more often connected to branch out of the fluid line. In this study, during operation, the flow of fluid is limited to reciprocal motion between the accumulators and the cylinder chamber. (Ijas 2007)

The dynamic response of a pressure accumulator is defined by the capacitance, as they act as gas springs. A transfer function of pressure accumulator with linearized friction is defined as:

$$\frac{Q_{acc}}{P_{acc}} = \frac{C_{acc}s}{\frac{s^2}{\omega_{acc}^2} + \frac{2c_m}{\omega_{acc}}s + 1} \tag{27}$$

Where Q_{acc} is the flow out of the accumulator, P_{acc} is the pressure at the accumulator inlet, C_{acc} is the accumulator capacitance, c_m is the accumulator damping coefficient and ω_{acc} is the accumulator specific angular velocity, which is defined as follows:

$$\omega_{acc} = \frac{1}{\sqrt{\dfrac{\rho C_{acc} l_{th}}{A_{th}}}} \tag{28}$$

Where ρ is the density of the hydraulic fluid, L_{th} is the length of the accumulator throat and A_{th} is the throat cross-sectional area. (Närvänen 2024)

3 Literature review

Many studies related to the tasks of vibration attenuation and adaptive vibration damping have been conducted. This chapter investigates prior studies on the subject and other relevant research.

Närvänen studied a system where a resonator consisting of a long pipe and a bladder accumulator was connected to a hydraulic cylinder to attenuate vibration. The system was both simulated and experimentally tested. The 80/125 hydraulic cylinder acting as a damper was vibrated by another hydraulic cylinder of same size, with the pistons of the cylinders connected to a steel sled. The accumulator used was a bladder accumulator with a nominal volume of 4 litres, and it was connected to the bottom of the damping cylinder with a pipe that was 2 meters long and had an internal diameter of 15 mm. Both cylinders were 80/125 It was found that at certain frequencies the resonator could improve the dynamic stiffness of the system by a factor between 4 and 10. On other vibration frequencies the dynamic stiffness was less than with the resonator disconnected. The simulated results were noted to show stiffness of around three times higher than the measured results. (Närvänen 2024)

The thesis of Sirviö investigated vibration damping with a variable-volume Helmholtz resonator connected to a four-chamber hydraulic cylinder. The resonator consisted of a pipe connected to a hydraulic cylinder, the piston of which could be held in place using brake pads gripping on the rod. The excitation for the vibration was implemented by using an eccentric motor in a test bench which restricted movement to exert a sinusoidal vertical force on the cylinder. Load was added on the test for additional inertia and downwards force. Tests were carried out with five different frequencies chosen within the theoretically determined natural frequency range of the system between 19 Hz to 35 Hz. Altogether, such tests were performed at seven different main cylinder positions and 19 different volumes for the resonator. It was found that in best cases the vibration amplitudes were reduced by almost up to 69 %, but that the resonator could also amplify the vibration by up to 78 % in the worst cases. (Sirviö 2022)

In Kela's dissertation, a variable volume Helmholtz resonator was used as well. The Helmholtz resonator consisted of a pipe and a hydraulic cylinder that formed the fluid volume. The volume could be controlled by actuating the cylinder piston, changing the cavity length. The goal of the study was to create a system that would adapt to damp vibration although the vibration varies. Both closed- and open-loop control was used to control the length of the cavity. This study also noted that the adjustable frequency band of the system was narrower than expected. Attenuation of 20 dB was reached between frequencies of 34.2 Hz and 38 Hz during open-loop experiments. Dissolution of air and variations in temperature were considered to cause the difference between theory and experimental tests. A notable difference to

Sirviö's work was that the cylinder piston was not locked in place, instead held by the pressure in the non-resonator side chamber and the cylinder sealings. However, the pressure of the system was very low at 3 bar, which could have negated any issues caused by this. (Kela 2010)

Lamsal's thesis investigated the effects of junction shape on the pressure losses in a hydraulic system under dynamic conditions. As the sharpness of corners and shape of the junction introduce turbulence and cause energy losses, the performance of damping components in a hydraulic system may be decreased due to junctions. In the thesis, a traditional T-junction, a conventional sharp-cornered Y-junction and a smooth Y-junction were tested under pulsatory and oscillatory flow. The junctions were fitted with three pressure transducers, with one transducer placed near each port. A multitude of tests under various conditions were carried out, including tests under oscillatory flow conditions. Oscillatory flow was achieved through excitation of a hydraulic cylinder piston connected to the piston of another cylinder which was in turn moved by allowing flow through a proportional control valve. It was found that the smooth Y-junction had lower hydraulic impedance. While there was evidence of the smooth junction moderating pressure fluctuation and maintaining more consistent, the overall effects were numerically small and not enough to justify its application in universally. (Lamsal 2024)

The study of Feng et al., focused on the modelling of stiffness characteristics of a hydraulic cylinder. A model, presented in equation 3, was developed based on previous studies on the subject. It was noted that older mathematical models neglected factors such as the air content in the hydraulic fluid, volume expansion of the cylinder barrel, and the effects of the hydraulic cylinder sealing. Experimental testing was performed. The setup used a loading cylinder and the experimental cylinder, which were installed on a test platform and connected to a trolley. While a model used for comparison showed errors of up to 40 % towards the start of the cylinder stroke, the error of the model introduced was under 10% at all measurement points, of which there were five in total. The study presents the level influence of various factors on the stiffness characteristics, with the most significant factor being the hydraulic fluid stiffness, above 70 % at all measurement points. The cylinder barrel expansion stiffness was shown to have a level of influence of approximately 10 %. It was noted however that the ratio of impact varies due to differences in cylinder sizes. (Feng, et al. 2017)

4 Methods

This section focuses on explaining the test setup and procedures, simulation models and the methods for evaluating the validity of the models. The simulation model is presented, followed by a description of the experimental test setup. A final subchapter is dedicated to detailing the test procedure and describing how the measurement data was processed.

4.1 Modelling

In the study a MATLAB Simulink model (Figure 7) was developed to simulate the stiffness of the system at various frequencies and cylinder piston positions.
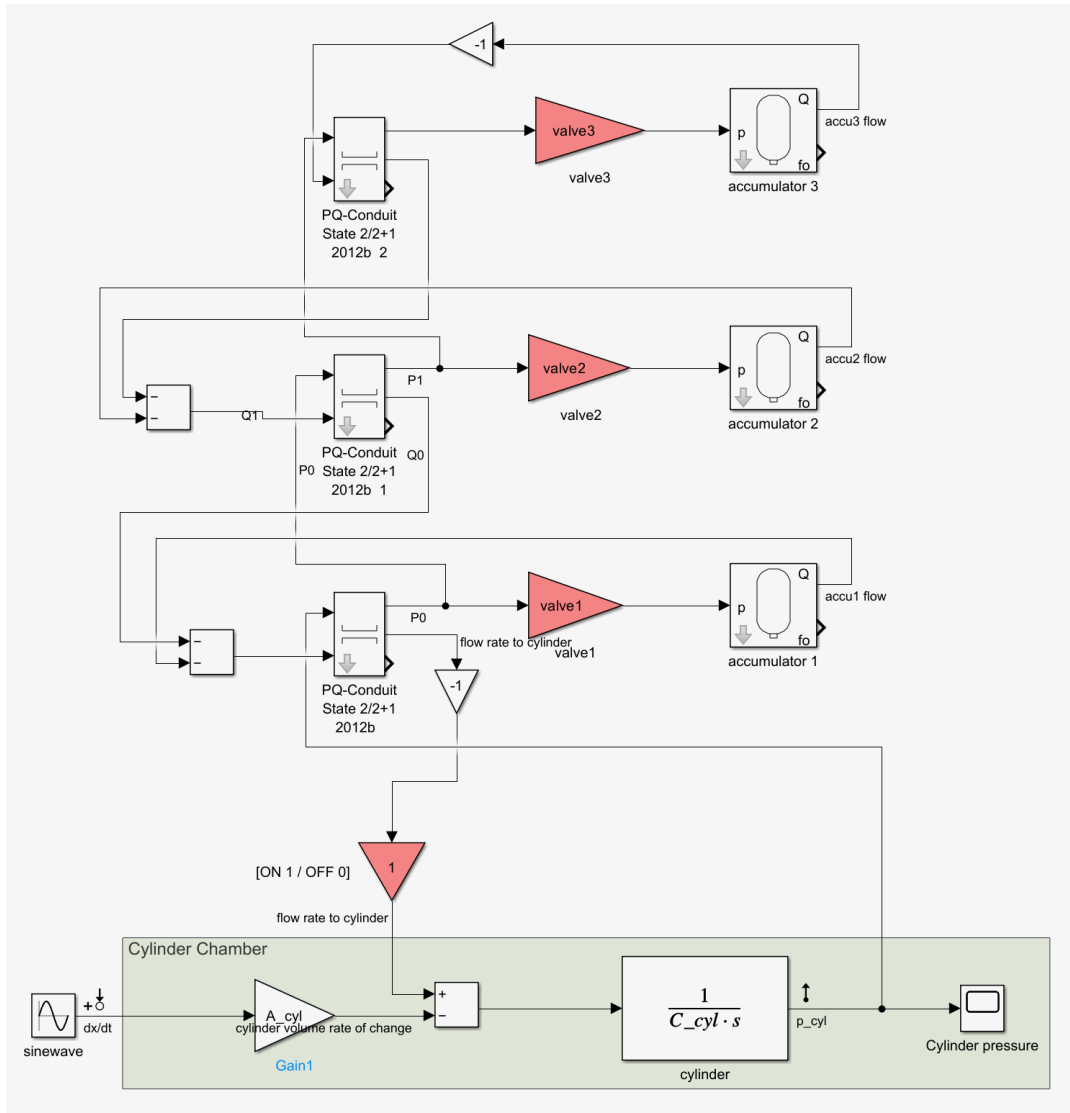
Figure 7. Simulink model of the damping system

The model has three PQ-conduit blocks which use the modal approxima-
tion method described in chapter 3.3.3 to simulate three pipes between the
cylinder chamber and the accumulators (Figure 8). The cylinder chamber
that is connected to the accumulators with pipes was simulated as the hy-
draulic capacitance of the chamber. The capacitance of the chamber was
changed in the MATLAB script, as well as the setting for the gain blocks to
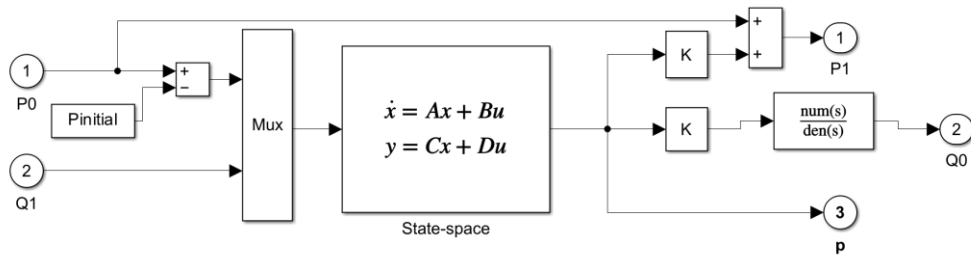disconnect the accumulator blocks from the model.

Figure 8. PQ-conduit block used in the system.

Subsystem blocks for accumulators were also used (Figure 9). Accumula-
tors were simulated as connected to the same pipe leading to the cylinder at
different lengths with equal spacing in between accumulators. Accumulators
were simulated as identical with equal charge pressures. The input of the lin-
earised system was the sinusoidal velocity. As the velocity is constant, the
cylinder pressure, which was used as the output, represents the amount of
force for effective piston area necessary to achieve the constant velocity os-
cillation.

$$\frac{C\_ha \cdot s}{1/(w_accu)^2 s^2 + 2 * zeta\_accu/w\_accus + 1}$$

Linear Accumulator Q/p

Figure 9. The accumulator subsystem consists of a transfer function pre-
sented in equations 27 and 28.

4.2 Experimental Setup

Testing was performed using a test bench with two hydraulic cylinders, one of which was used to exert the excitation force on the proposed damper. The excitation cylinder could be made to oscillate at a constant displacement, which would make the comparison between the model and test results easier. The resonator consists of hydraulic cylinder that is connected through a 12-meter-long pipeline to a pressure accumulator (Figure 10).
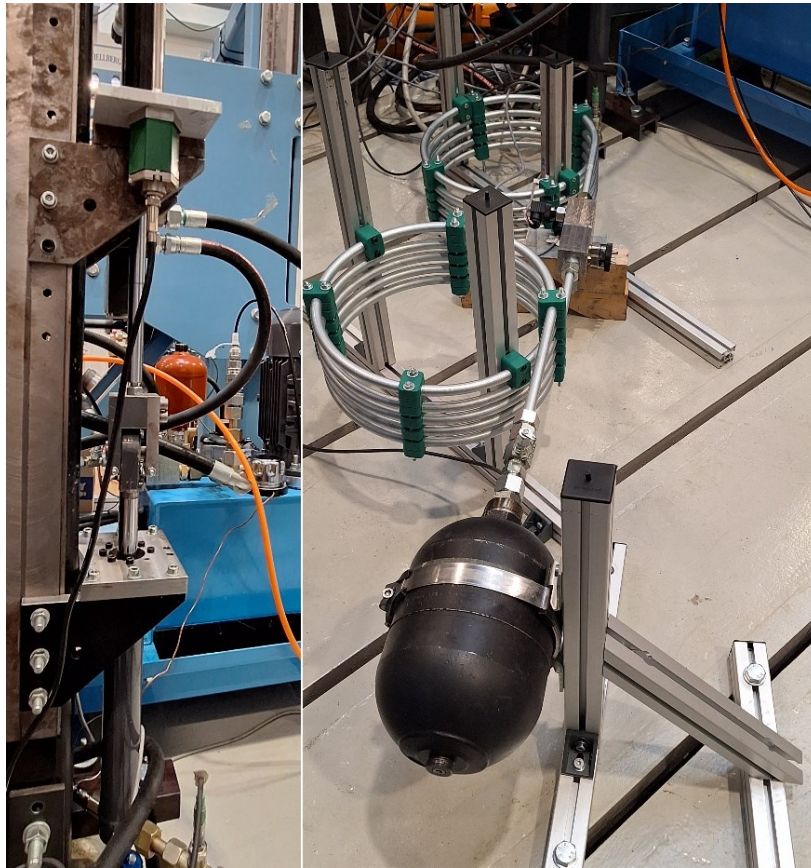

Figure 10. The upper hydraulic cylinder provides excitation to the system (left) while the lower cylinder connects to the damping system with accumulator and two coiled pipes (right).

Due to limitations in testing space the fluid line consists of two 6-meter-long coiled pipes. The resonator parts were supported by slotted aluminium extrusions due to availability and ease of construction and adjustment. The pipes were installed to rise towards the accumulator to facilitate removal of air from the system. System pressure during tests was 40 bar. The following subchapters describe some of the key components of the system.

The excitation cylinder, which was used to provide vibration for the test system, was a symmetrical cylinder. It was actuated by a proportional control valve and could be made to vibrate at a somewhat constant displacement

using PID control. The resonator cylinder was a differential cylinder, the rod of which was connected to the rod of the excitation cylinder. The maximum stroke of the resonator cylinder was 220 mm, and the inner diameter was 40 mm. The chamber with no rod was connected to the resonator.

The pressure accumulator used in the test was a membrane accumulator, with a volume of 3.5 litres (Figure 11). The gas pressure of the accumulator was set to 30 bar, 75 % of the system pressure.
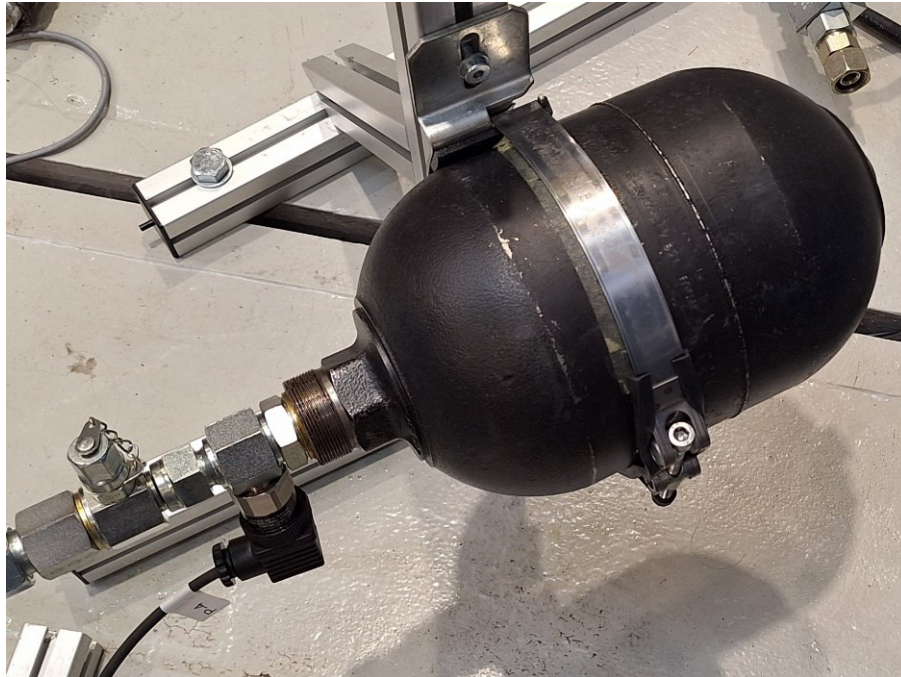

Figure 11. Pressure accumulator used in the system.

The test setup had sensors for the cylinder chamber pressure, accumulator pressure and the pressure in the middle of the pipe leading to the accumulator.

For measurement of the cylinder piston position a magneto strictive position sensor was used, as one was readily available on the test bench. The sensor used had a 16-bit resolution and a minimum repeatability of ±3 μm (Santest Co., Ltd. 2023). It was used to measure and control the vibration of the cylinder and allowed positioning to measurement points along the cylinder stroke. The sensor can be seen, attached to the test bench, on the upper left in Figure 10.

Three pressure sensors were used in the test setup, as seen on the system diagram (Figure 12). A sensor was placed at the resonator cylinder, another on a manifold connecting the two coiled pipes and the last was placed at the pressure accumulator entrance. Of these the most significant was the cylinder pressure, as the simulation models used cylinder pressure to express the system stiffness. The other sensors were used to validate pressures seen in the model and for estimation of possible pressure losses or other differences

to the model. All pressure transducers had a recommended range of 0 to 100 bar and a ±0.5 % to full scale accuracy (Trafag AG 2024) (Trafag AG 2024). The cylinder pressure sensor can be seen in Figure 10, connected to the cylinder on the side opposite to the resonator pipe.
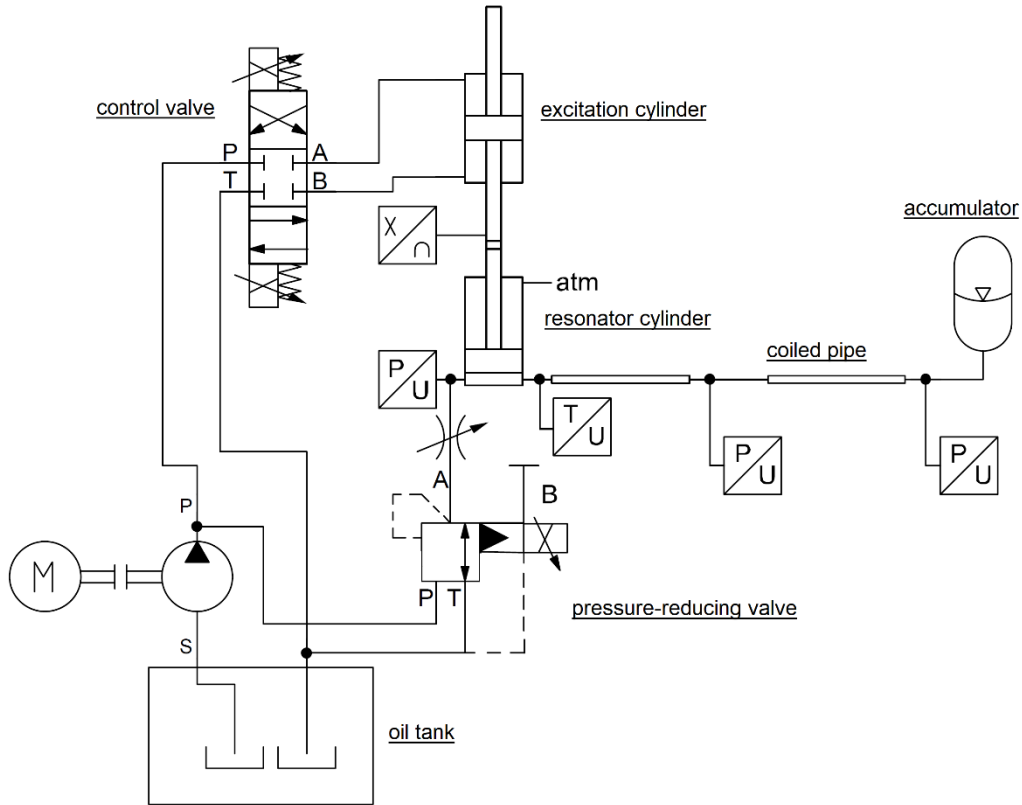

Figure 12. Diagram of the test setup.

A temperature sensor was used in the system to observe the temperature on the test bench side. This was used to try and set the temperature near 40 degrees Celsius. However, as there was no flow through the piping, temperatures on the accumulator end were cooler. Trying to warm the entire resonator by allowing flow was deemed too arduous and ultimately unnecessary. Even temperature would be more easily achieved by warming the pipes with radiators, for instance. The pump used in the test system also had a thermometer as part of the oil tank, and the system had a water cooling system to regulate the temperature on the pump side.

4.3 Testing procedure

Four cylinder positions with equal increments were used in the test. As the test bench limits the movement of the piston, only a part of the cylinder stroke could be measured. The lowest resonator cylinder piston height where

measurements were performed was approximately 92.5 mm and highest 212.5 mm. No tests were performed with the resonator disconnected.

The test procedure itself was conducted with a frequency sweep, where the vibration started at 7 Hz and went up to 40 Hz over a span of around 140 s. The system had PID control to keep the vibrations at an amplitude of 0.3 mm. Due to higher frequencies, above approximately 30 Hz, the proportional control valve used to vibrate the excitation cylinder couldn't let enough flow in and out of the cylinder to move it at the desired amplitude. The test was repeated three times at each cylinder position. Data was gathered at a sample rate of 1000 Hz.

Data processing was done entirely using MATLAB. To ease processing of measurement data, the datasets of the three measurements were cut to the same length. First, approximate limits of piston velocity were used to determine if the test had begun, or ended, to remove the data from outside the test procedure. As this resulted in the sizes being quite close, a few rows of data could be removed from the end of the datasets. This was justified as the 35-40 Hz was considered outside the frequency band of interest in this study, with the resonator dimensions chosen to give a pressure oscillation peak around 20-30 Hz band. Additionally, as explained previously, at higher frequencies of the sweep the valve caused issues with control, possibly compromising the quality of the measurements at the end of the test dataset.

This allowed easier use of Fast Fourier Analysis and finding the averages of the test results. Fast Fourier analysis was used to analyse the datasets in 10000 data point sets, which corresponded to 10 seconds of time during the test. The average of the three measurements at each set was calculated. The highest amplitudes for a frequency were taken from the sets to combine them into one array of amplitude data.

5 Results

In this chapter the results are presented. First, simulation results are presented, after which the experimental results are shown. Finally, the results are compared and discussed.

5.1 Simulation results

The simulation model was used to create a 3D surface plot that shows the best possible stiffness of the system of the nine different valve configurations, as each accumulator could be disconnected from the system.

Figure 13 presents a surface plot of highest pressure amplitudes that is coloured to show the accumulators connected to the system. As there are three accumulators which can be connected to the system, there are eight different combinations. The input values of the surface plots are 1 meter per second for velocity input and one meter for displacement input.
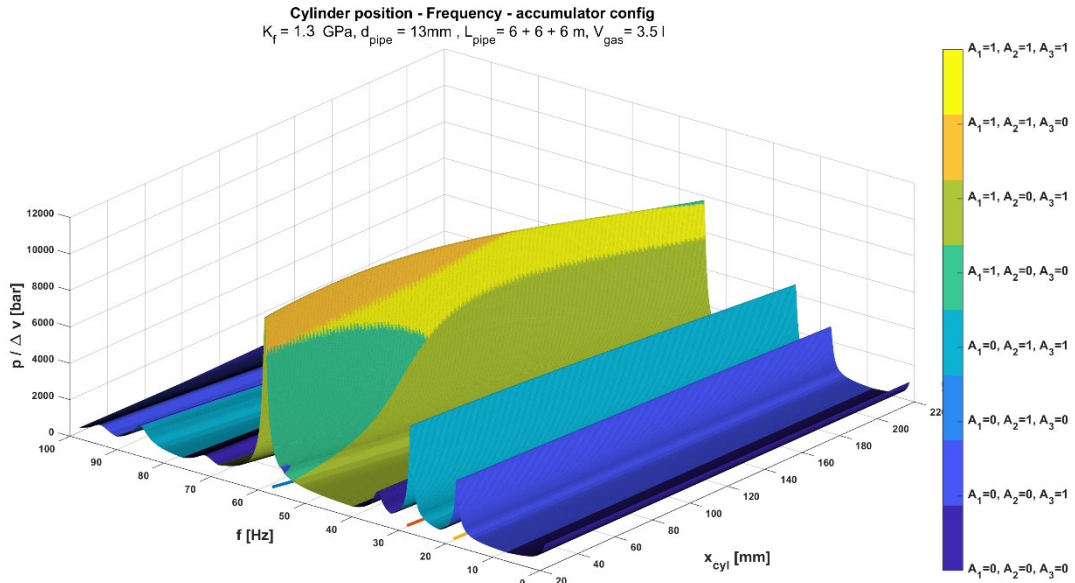
Figure 13. Example of a surface plot with best possible stiffness. The colour bar on the right shows which accumulators are connected (1) and disconnected (0), with A_1 being the accumulator closest to the cylinder.

In initial simulations, the bulk modulus was assumed to be 1.3 GPa. This was later estimated to be lower, due to lower working pressures and possible air trapped in the experimental system. As the simulation model input was set to the piston velocity, the resulting pressures were multiplied by $2\pi f$ so the input would correspond to displacement. Viscosity for simulations was initially 32 cSt. The system was simulated with velocity as the model input

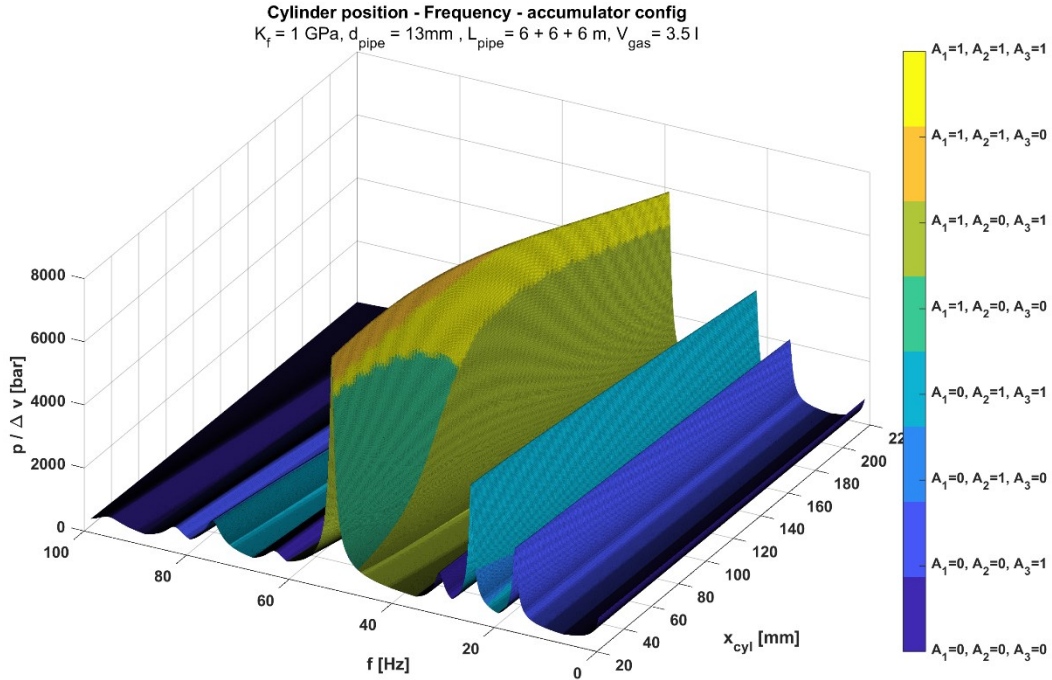(Figure 14) and results were converted to use a vibration displacement input (Figure 15).

Figure 14. Initial simulation results for highest chamber pressure amplitude, with a velocity input.
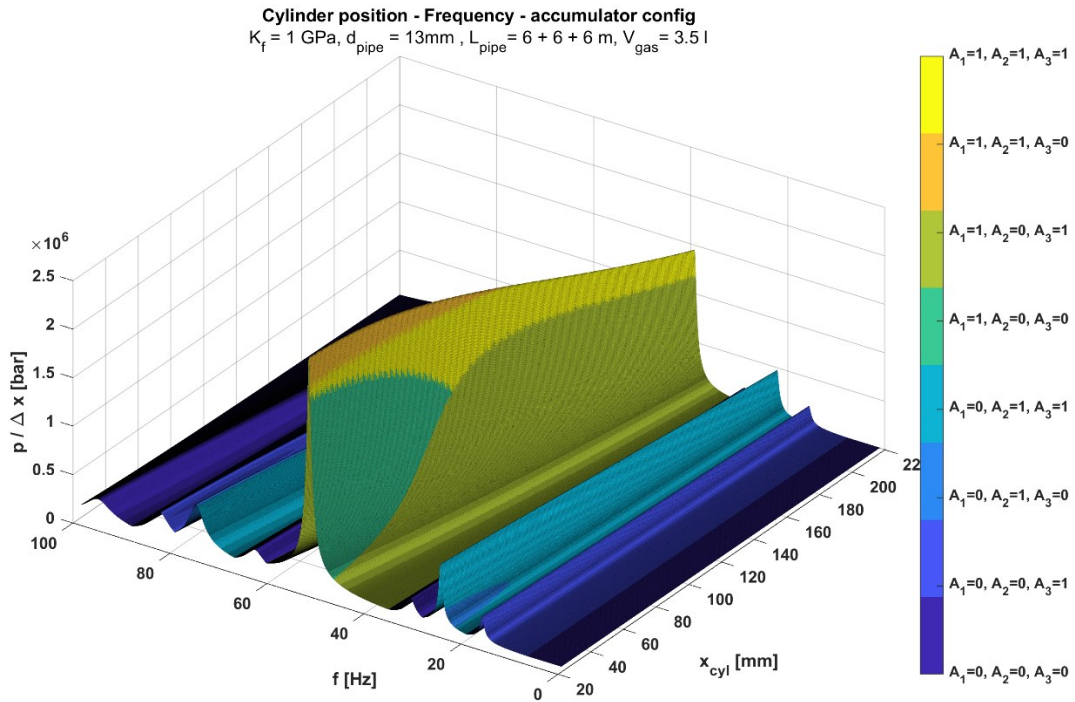

Figure 15. Initial simulation results for highest chamber pressure amplitude, with a displacement input.

From initial results, the plot seen in Figure 15 shows that the 12-meter pipe would lead to a ridge (coloured teal in the figures) of highest pressure amplitudes between approximately 20 and 25 Hz across the cylinder stroke. This result led to the use of two 6-meter-long coiled pipes the test system, but the system was also simulated with 6 and 18 meters of pipe.

The maximum stiffnesses form ridges. As the piston position increases, and cylinder chamber volume increases, the frequency of the peak stiffness decreases, as does the stiffness itself. This is most clearly seen in the highest ridge at the middle of the plot, formed by results from the four configurations where the closest accumulator, at 6 meters of fluid line, is connected. Increasing pipe length appears to reduce this effect. A longer pipe also causes peak stiffnesses at a lower frequency but decreases the maximum stiffness. Lower pressure peaks can be observed on higher frequencies with accumulator configurations, most visible perhaps with accumulators 2 and 3 connected.

Figures 14, 15 and 16 show that the accumulator at the nearest fluid line distance from the cylinder has a dominating effect on the frequency and amplitude of peak stiffness, and connection of additional accumulators at longer pipe lengths has a very small effect.
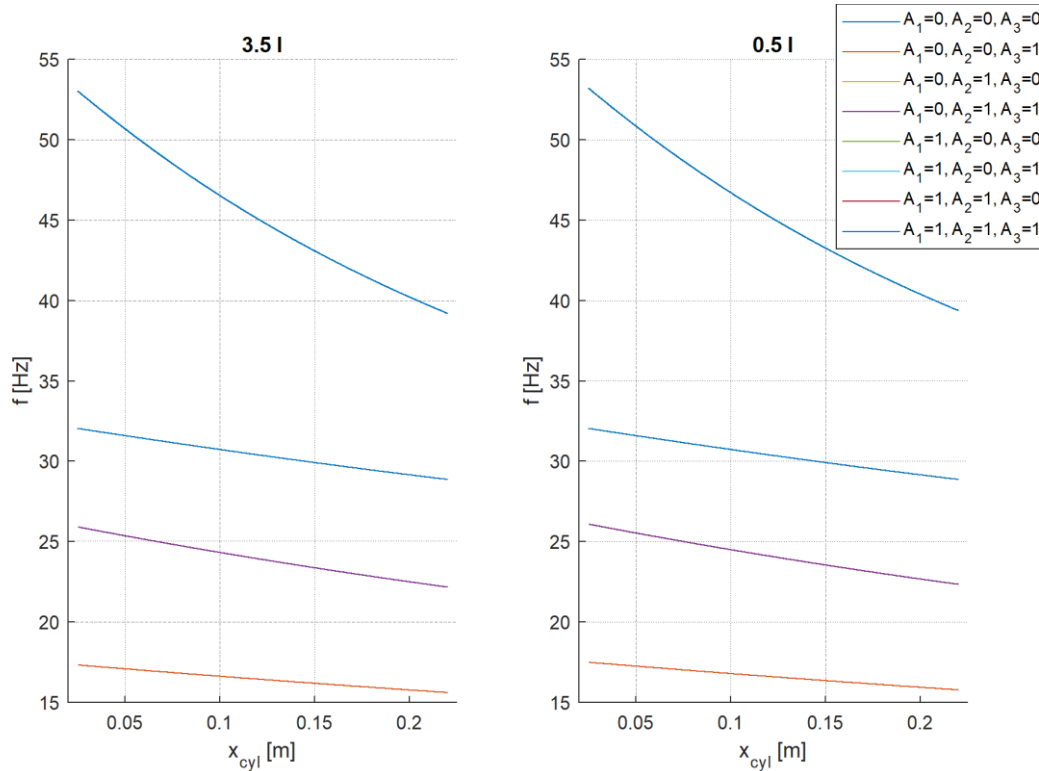

Figure 16. The frequency corresponding to each configuration's maximum stiffness. The 3.5 l accumulator is compared against a 0.5 l accumulator.

The highest curve in the above figure represents the settings where the 6-meter accumulator is connected. The second highest curve is in fact the

system with all accumulators disconnected. From previous figures, however, the stiffnesses at this setting are much lower compared to others. The pipe would effectively act as a T-pipe and have a much higher optimum frequency. This is the pipe's optimal frequency curve for stiffness within the simulation limits of 1 Hz and 100 Hz. The lowest represents only the furthest accumulator being used. The figure shows the system's frequency curves for maximum stiffness, or the top of the ridges seen in Figure 15. Notably when zoomed in very closely (Figure 17) accumulators further than the nearest connected accumulator make little difference to the frequency of optimal stiffness. For Figure 16 system was simulated with 0.1 mm resolution for the cylinder piston position, and 0.01 Hz resolution for the frequency. While most simulations used a 1 mm resolution for piston position instead, this one was performed with higher resolution.
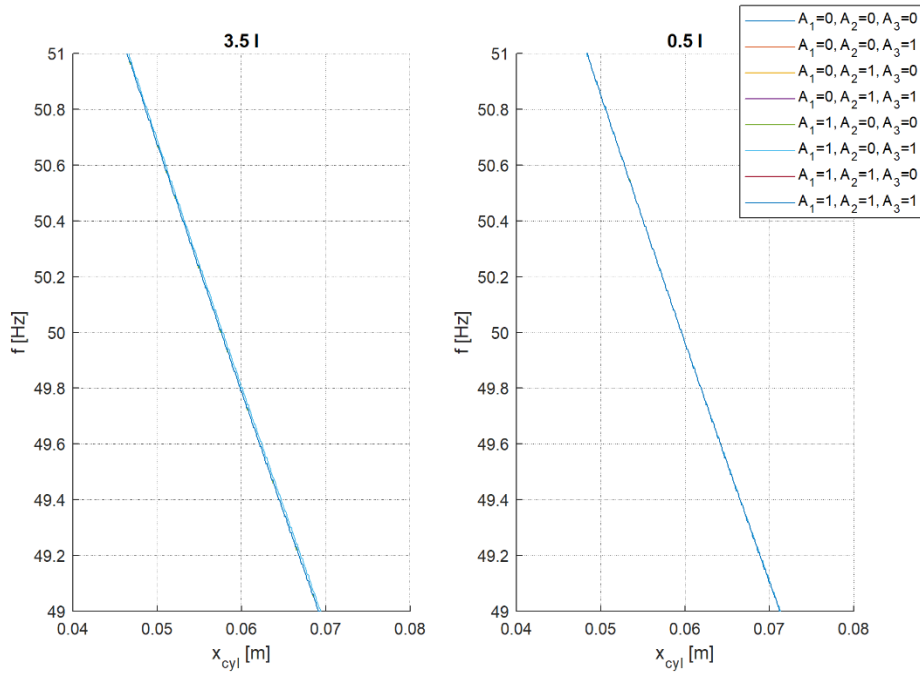

Figure 17. The simulation plots of zoomed in to show the small difference between accumulator configurations where the nearest accumulator is connected.

Based on earlier simulations it appeared that lower accumulator volumes, less than one litre, would lessen the dominance of the first accumulator and show more divergence caused by further accumulators. Further simulations showed the difference is in fact very small, and that the 0.5 litre accumulators have a visibly smaller divergence in the figure, although the simulation resolution is likely not enough to verify this. Greatest difference in optimal frequency between the configurations seen in the figure was 0.01 Hz. Figure 16 and Figure 17 also show that the accumulator size has a slight effect on the optimal frequency, a higher volume leading to a slightly lower frequency.

5.2 Test results

The measured cylinder chamber pressure amplitudes are seen in Figure 18. The four plots present the averaged results of the fast Fourier transforms of the three tests performed at each measurement point.
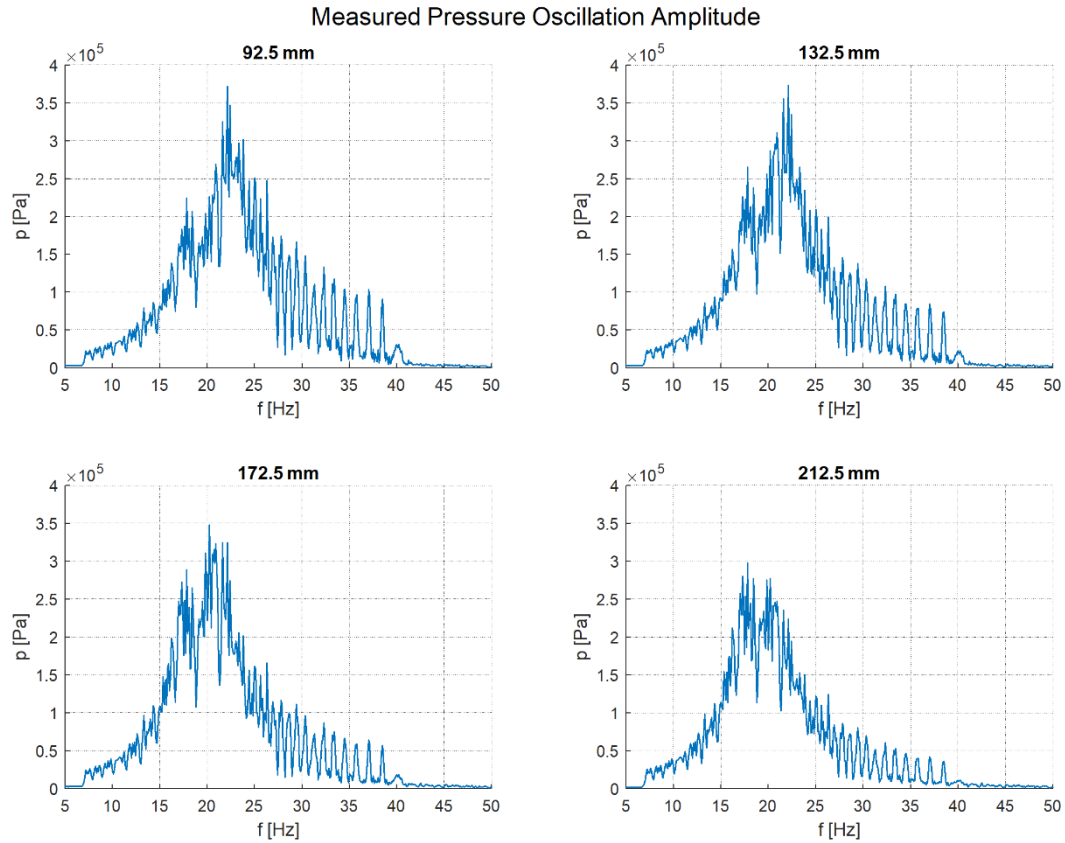

Figure 18. Measured cylinder pressure oscillation amplitudes at the four measurement points.

From the plots it is seen that maximum and overall pressure amplitude decreases towards the end of the cylinder stroke. There is a smaller, or in the case of the furthest measurement point, equal or even larger summit before the main frequency peak. The end of the has multiple smaller peaks, which may have been due to chosen data processing methods. It could also be caused by the inability of the system to oscillate at the desired constant displacement. However, these peaks are also seen in the curve for measured vibration amplitude (Figure 19).
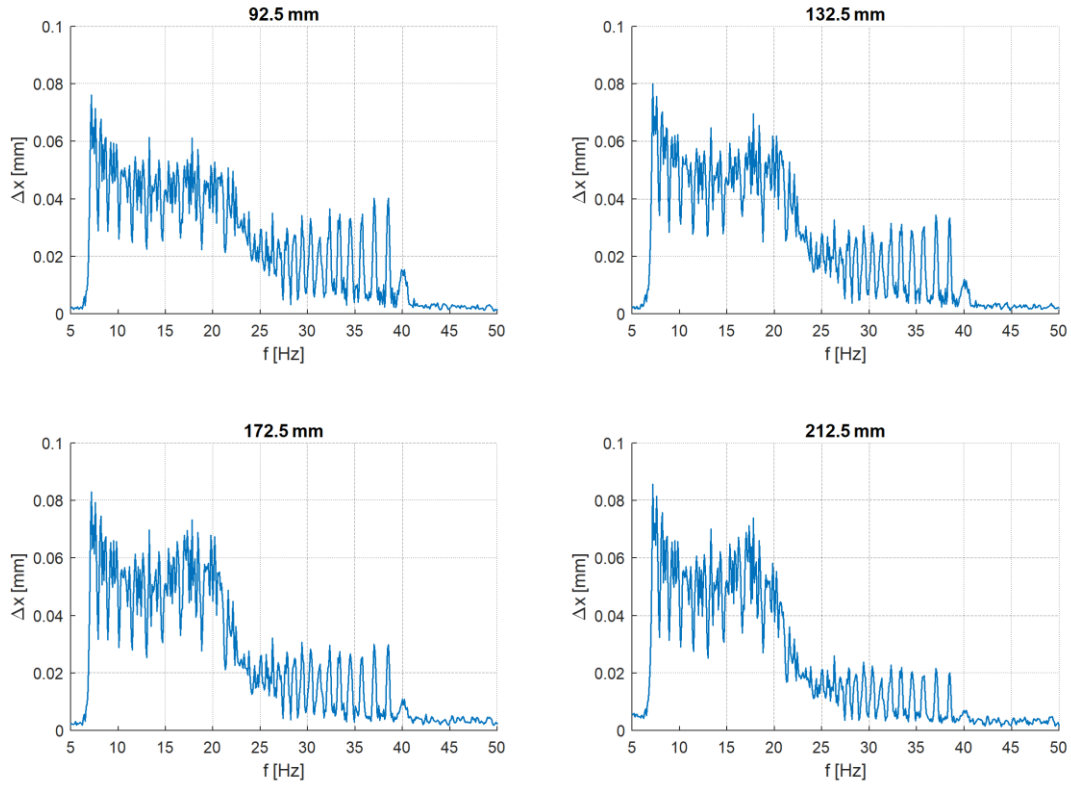
Figure 19. Measured vibration amplitude. The data was processed in the
same way as the pressure data.

The vibration amplitude appears to be much lower than the expected 0.3 mm amplitude. There is also a considerable drop in the vibration amplitude around 20 Hz, which appears to become more drastic as the piston is extended. The valve was expected to have with vibrating the cylinder at a constant displacement amplitude but the frequency at which the drop occurs suggests that the resonator begins to have a damping effect before the limitations of the valve are expected to affect performance.

The pressure oscillation at the pressure accumulator entrance were also measured (Figure 20). The accumulator pressure is at least 100 times lower than the cylinder pressure, and like the cylinder pressure, becomes lower as the piston is extended. Peak pressure oscillations occur near the same frequencies as in the cylinder chamber pressure, but the peaks are less pronounced, at least with less chamber volume.
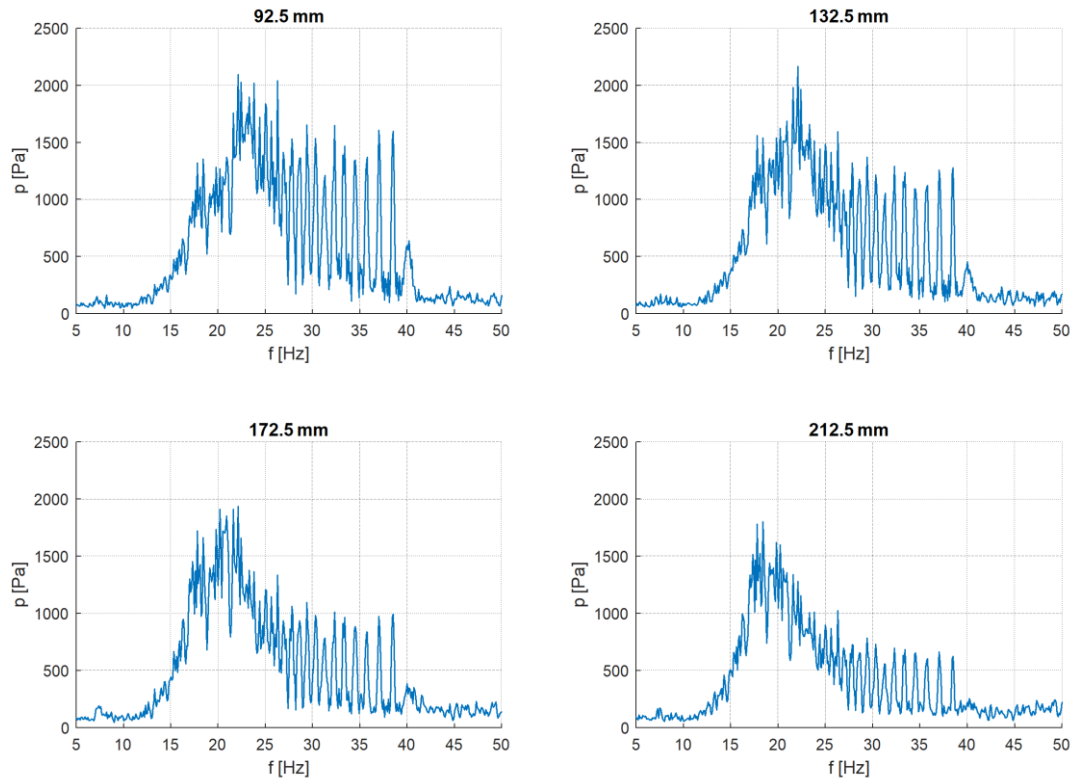
Figure 20. Measured accumulator pressure amplitude.

5.3 Comparison and adjustment of model parameters

The measured pressure was compared to the simulation model. As the simulation model used an input of the piston velocity, pressure comparison required conversion of the simulation results. The simulation was multiplied, or given the input, of the displacement amplitude of the tests, multiplied by $\pi * f$. Another curve used the average of the measured displacement between the band 7 - 40 Hz, the frequencies that were used in the test sweep, instead of the displacement amplitudes corresponding to each frequency. While the test amplitudes were otherwise quite close, the initial simulation, on which the construction of the test setup was based, was inaccurate in the prediction of peak pressure amplitude frequency, and the measured pressure peak was much lower in amplitude compared to the simulated peak. Simulation used viscosity of 32 cSt and fluid density of 870 kg/m³. These results can be seen in Figure 21 and Figure 22. The simulation results used in the comparisons only used data from the simulation where the 12 meter fluid line length accumulator was connected.
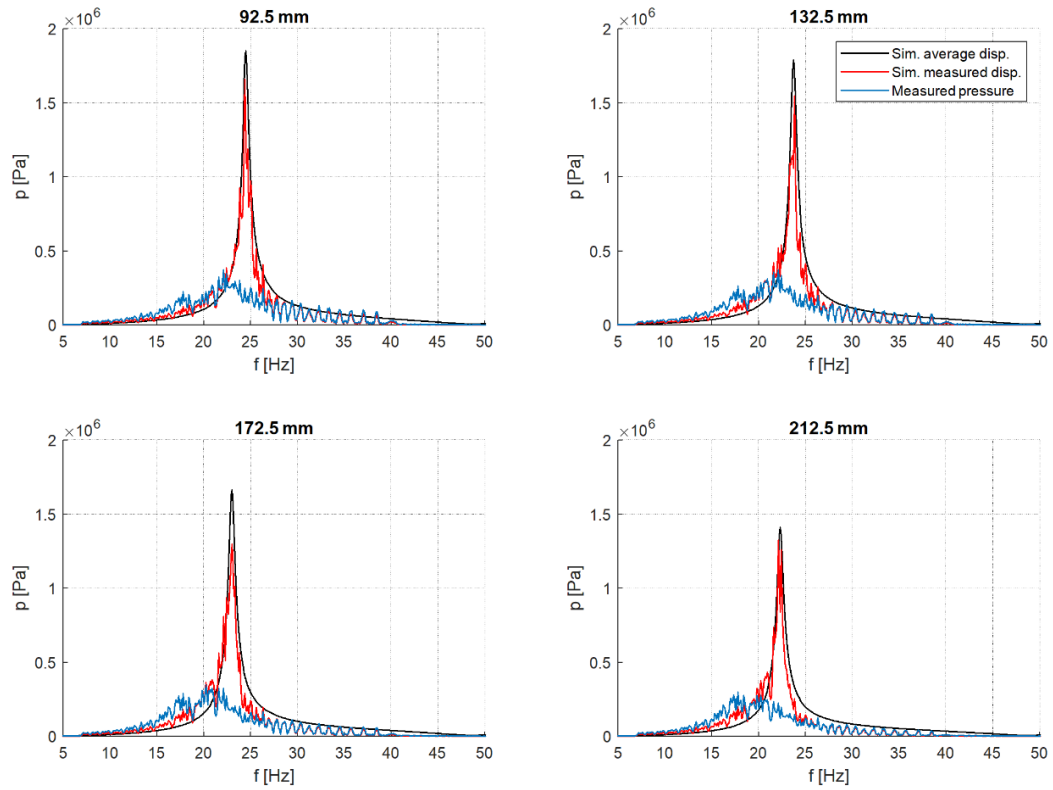
Figure 21. Simulation results scaled using measured displacement for comparison with measured pressure amplitude.

In the above figure, the simulation results are multiplied by the FFT results of measured displacement. A second set of plots was made where results are scaled to the simulation by dividing measured pressure with displacement.
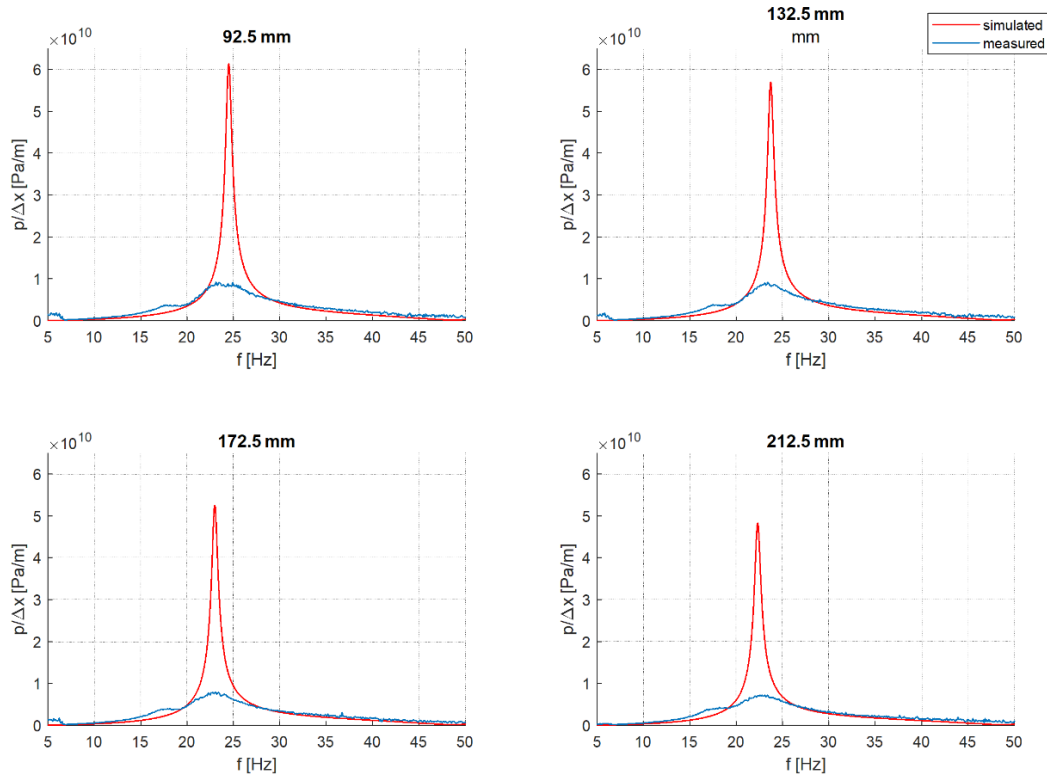
Figure 22. Measured pressure scaled with displacement to compare against simulation.

The peak stiffness of the measured system is far lower than the simulated result, but its frequency is close. Possible reasons for loss of stiffness include losses caused by friction, leakage and other factors. Part of the energy may have also been transferred to the resonator's structures, as strong vibrations were observed in the pipe supports during testing.

The measured accumulator pressure was compared to the measurements (Figure 23). The simulation output was changed to the pipe model between the first and second accumulator and the simulation was run with only the accumulator at 12 meter fluid line length connected.
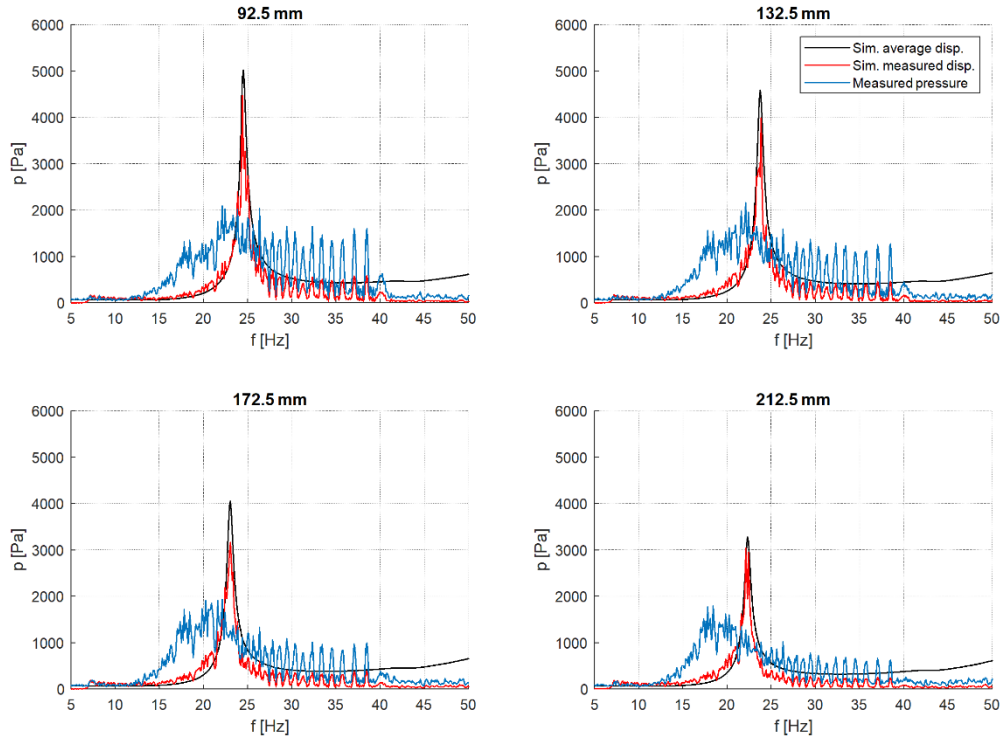
Figure 23. Accumulator pressure compared to simulations scaled using displacement.

The simulated accumulator pressure is lower away from the peak, and the simulated peak values are at least double the measured value. Overall, however, the accuracy of these results is less relevant, and the important part is that the scaling is close enough, meaning that there are no major issues with the model's accumulators. The measured pressure has a less pronounced peak, and this could be caused by damping and friction losses.

Overall, the simulation results appear to follow the measured results best after the peak. Before the peak, the measured pressure's rise is slightly steeper than that of the simulation, which could however mean that the measured peak is offset in favour of the simulation by some phenomenon occurring at approximately 17 Hz, causing the rise to halt momentarily.

Two variables were considered. There was some uncertainty to the viscosity and the bulk modulus of the fluid used, and how the effective values of these differed from theory. Temperature across the system was not constant, and pressure oscillation could affect the bulk modulus as well. In addition, the helical shape of the resonator pipes could have given the fluid more effective viscosity. Further simulations showed that the peaks were of more similar size with a viscosity of 128 cSt. The pressure of the overall system (40 bar) was also considered, as it could have caused a lower than typical effective bulk modulus. In Figures 24 and 25 the kinematic viscosity was quadrupled at 128 cSt.
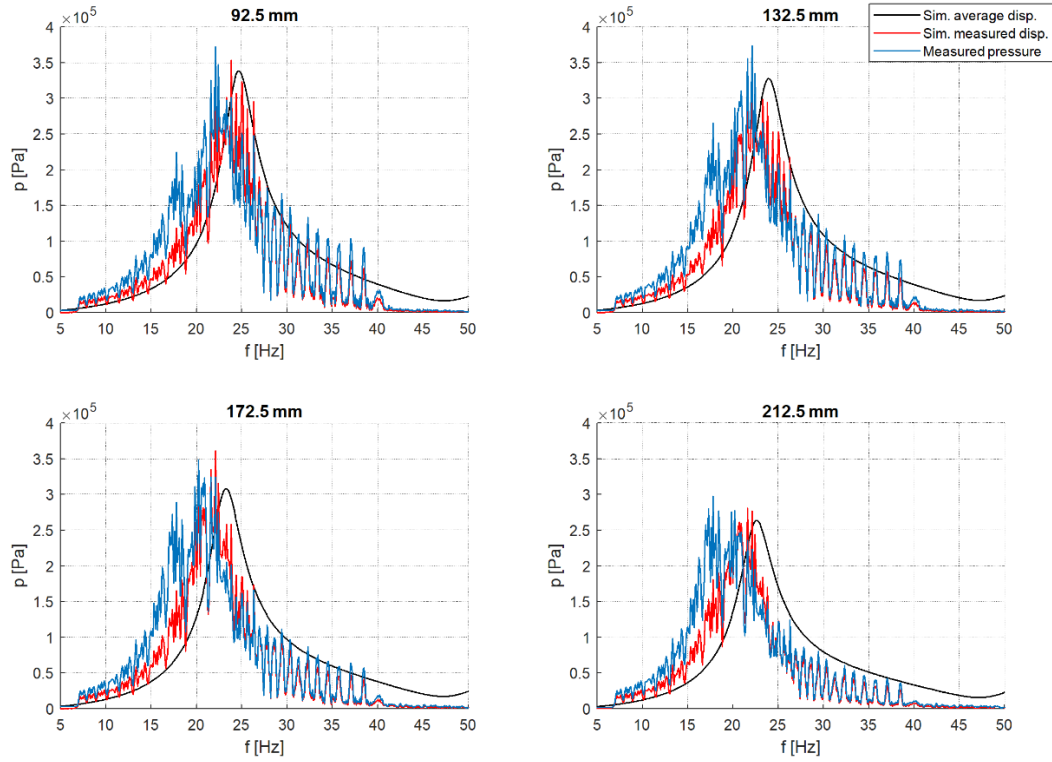
Figure 24. Simulation results with 128 cSt viscosity scaled with measured displacement and compared to measured pressure amplitude.
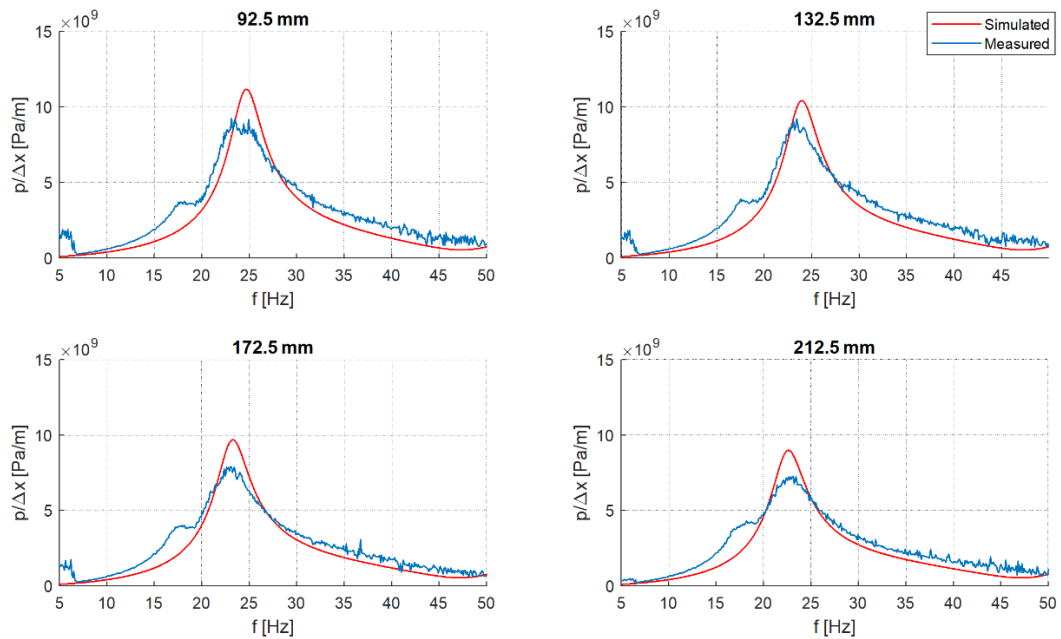

Figure 25. Simulation results with 128 cSt viscosity compared to measured pressure amplitude scaled by measured displacement.

From the figures on the previous page, it appears that the measured pressure drops slightly more compared to the simulated results as the piston is extended, increasing chamber volume. From a closer view it's easier to observe that the simulated peak's frequencies match better towards the end of the cylinder stroke. The decreased values of the simulation graph appear to match worse with the curve outside the peak compared to the earlier results, however. For instance, in the 212.5 mm curve, the simulated pressure to displacement becomes lower than the measured values at approximately 25 Hz, while in the initial tests this occurs closer to 27 Hz, and the simulation follows the remaining test results closer. A final surface plot, with a displacement input, of the 128 cSt simulation is seen in Figure 26.

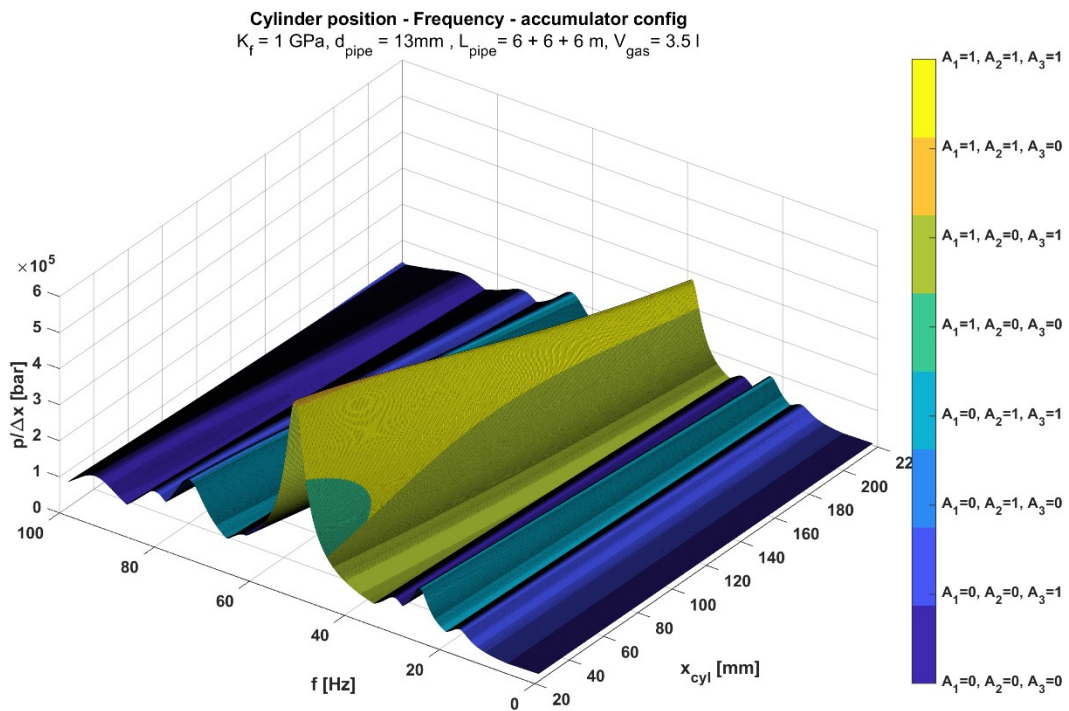Figure 26. Surface plot of the pressure amplitude at 128 cSt effective viscosity with displacement input.

The effects of added viscosity can be easily seen in the mostly yellow ridge formed by the accumulator configurations where the accumulator at fluid line distance of six meters is active. Compared to Figure 15, the stiffness is not only overall lower, but also drops more steeply towards the end of the cylinder stroke.

6 Discussion

There was some deviation between the simulated and measured results. The experimental test setup was constructed with a coiled pipe instead of the simulated pipes, which were straight, due to space restrictions. While this allowed for testing the system at the desired pipe length, the coiled pipes likely affected the test system's performance and caused uncertainty in the assessment of the model.

Only a system with a single pressure accumulator was tested in this study. Because of this, many of the phenomena present in the simulation models could not be experimentally confirmed. These include the dominance of the first connected accumulator from the fluid line in defining the frequency and amplitudes of the peak stiffnesses across the cylinder stroke, and accuracy of the model across a multitude of fluid line lengths.

There are many other phenomena that could be considered in future simulations of the problem that were not included in the model developed in this study. These would include the expansion of the pipe under pressure or due to heat expansion and the pressure losses as fluid moves through the inlet of the hydraulic cylinder, the latter of which may have only a small effect, however. The effects of stick-slip and elastic deformation of the sealings in the cylinder were ignored, which could have been relevant due to the measured amplitude of vibration. Other causes for inaccuracies include mechanical vibration of the resonator and air content of the fluid.

The temperature of the system was mostly ignored in this study, and the system was not of uniform temperature, decreasing towards the accumulator end. If it was needed, the most likely solution would have been to install heating coils around the system, as heating the system by fluid flow could still allow the accumulator side to cool down during operation, when flow through can't be allowed. Additionally, the temperature of the accumulator, which could also rise during prolonged operation, was not measured.

While the research presents a method for pressure damping, further research with experimental testing of the system simulated in the study would be needed to confirm its usefulness in practice. The simulation model presented optimistic results in terms of stiffness, and while added viscosity was able to compensate for this somewhat, future models would have to account for multiple other sources of pressure losses, and other factors which affect the stiffness of the hydraulic cylinder system. The addition of heating coils or achieving constant temperature through other methods would ease assessment of simulation accuracy by eliminating unknown factors in future research. Another opportunity would be to simplify the test setup by using straight pipes instead of coils.

7 Conclusion

In this study, the modelling and simulation of a hydraulic damping system using a resonator multiple pressure accumulators were studied. The main research question was how well the damping system could be simulated to dimension the system and predict its behaviour. The system's optimal frequency could be predicted well, but stiffness was much higher in simulations.

Using a resonator, reflective damping of vibration of a hydraulic cylinder can be achieved by maximizing pressure oscillation which increases stiffness significantly. This peak of pressure oscillation is achieved by finding the resonance frequency. In the system, this frequency can be adjusted by changing the dimensions of the accumulator, pipe and cylinder. As the cylinder in this research problem would be actuated, the cylinder volume varied, causing changes in the dynamic behaviour of the system.

A model was made in MATLAB Simulink for a system with three accumulators. It was found that increasing the pipe length decreases the maximum stiffness. The fluid lines were simulated using modal approximation. While the cylinder volume was simulated as a volume of fluid with compressibility, the pressure accumulator model also accounted for the accumulator's damping effects.

From simulations, it was found that as the cylinder chamber's volume increases when the cylinder is extended, the frequency of peaks in pressure oscillation amplitude lowers slightly, as does the maximum amplitude. This effect decreased as pipe length increased. The increase of pipe length also lowered the frequency of the pressure peak but decreased maximum stiffness. It was found that the accumulator nearest to the cylinder in fluid line length had a dominant effect on the dynamic characteristics of the system, although this could not be experimentally confirmed.

Experimental testing was conducted with a single accumulator with twelve meters of fluid line between the accumulator and cylinder. The system was excited with a constant displacement vibration with a separate hydraulic cylinder. Tests showed the experimental setup had a much lower maximum pressure amplitude which could have been caused by use of coiled pipes instead of straight or air content in the fluid. Viscosity in the simulation was increased to simulate added pressure losses and inertia that may have been caused by the coiled pipe structures.

Additional simulation showed quadrupled viscosity having pressure amplitudes significantly closer to those of the measurements. However, due to relative simplicity of the model, further research with more detailed modelling, especially in terms of possible pressure losses should be considered in the future. Additionally, experimental testing of the simulated system with multiple accumulators connected to a single pipe at various lengths is recommended to test the concept presented in the simulation model.

References

Feng, Hao, Qungui Du, Yuxian Huang, and Yongbin Chi. 2017. "Modelling Study on Stiffness Characteristics of Hydraulic Cylinder under Multi-Factors." *Strojniški vestnik - Journal of Mechanical Engineering* 63 (7-8): 447-456.

Hružik, Lumìr, Martin Vašina, and Adam Bureček. 2013. "Evaluation of Bulk Modulus of Oil System with Hydraulic Line." *EPJ Web of Conferences* 45.

Ichiryu, Ken. 1973. "Surge Absorption by Accumulator : Study in the Case of Air Content in Oil." *Bulletin of JSME* 16 (92): 319-327.

Ijas, Mika. 2007. *Damping of low frequency pressure oscillation.* Dissertation, Tampere, Finland: Tampere University.

Jorkama, Marko. 1996. *On The Winder Vibration Analysis.* Licenciate's Thesis, Järvenpää, Finland: Helsinki University of Technology.

Kela, Lari. 2010. "Adaptive Helmholtz Resonator in a Hydraulic System." *International Journal of Mechanical and Mechatronics Engineering* 4 (8): 684-691.

Kim, Sunghun, and Hubertus Murrenhoff. 2012. "Measurement of Effective Bulk Modulus for Hydraulic Oil at Low Pressure." *Journal of Fluids Engineering* 134 (2).

Kinkler, Bernard G. 2011. "Fluid Viscosity and Viscosity Classification." In *Handbook of Hydraulic Fluid Technology*, 181-218. Milton, United Kingdom: Taylor & Francis Group.

Lamsal, Sanyog. 2024. *Impact of smooth flow path junctions in resonator systems on hydraulic cylinder damping performance.* MSc Thesis, Espoo: Aalto University.

Lu, Heikki. 2021. *Stiffness characteristics of hydraulic cylinder system subjected to dynamic loading.* Espoo, Finland: Aalto University.

Mäkinen, Jari, Robert Piché, and Asko Ellman. 2000. "Fluid Transmission Line Modeling Using a Variational Method." *Journal of Dynamic Systems Measurement and Control* 122 (1).

Mishra, P., and S.N Gupta. 1979. "Momentum Transfer In Curved Pipes. 1. Newtonian Fluids." *Industrial Engineering Chemistry Process Design and Development* 18 (1): 130-137.

Mobley, R. Keith. 2000. *Fluid power dynamics.* Boston: Newnes.

—. 1999. *Vibration Fundamentals, 1st ed.* Elsevier Science & Technology.

Närvänen, Ville. 2024. "Experimental bladder accumulator based passive resonator." *GFPS PhD Symposium.* Hudiksvall.

Ortwig, Harald. 2005. "Experimental and analytical vibration analysis in fluid power systems." *International Journal of Solids and Structures* 42 (21-22): 5821-5830.

Owen, William Scott. 2001. *An investigation into the reduction of stick-slip friction in hydraulic actuators*. Vancouver: University of British Columbia.

Randall, Robert Bond. 2021. *Vibration-based condition monitoring: industrial, automotive and aerospace applications*. John Wiley & Sons.

Santest Co., Ltd. 2023. *Introduction of product | Santest Co., Ltd. that has magnetostrictive displacement transducer*. Accessed March 6th, 2025. https://www.santest.co.jp/en/product/series/all_in_one/gyse-a_probe_1.php.

Sirviö, Olli-Eemeli. 2022. "Vibration control of a four-chamber hydraulic cylinder system with a variable volume Helmholtz resonator." Espoo: Aalto University.

Song, Hongqing. 2018. *Engineering Fluid Mechanics*. Singapore: Springer.

Sun, Shuihui, Jiahao Liu, Ruili Sang, and Kang Zhao. 2022. "Experimental study of flow friction behavior in coiled tubing." *Energy Reports* 8 (12): 187-196.

Trafag AG. 2024. *EPI 8287*. Accessed March 17, 2025. https://www.trafag.com/en/epi-8287-industrial-pressure-transmitter/.

—. 2024. *NAT 8252*. Accessed March 17, 2025. https://www.trafag.com/en/nat-8252-industrial-pressure-transmitter/.

Watton, John. 2009. *Fundamentals of fluid power control, 1st ed*. Cambridge, New York: Cambridge University Press.

Xiao-Ming, Wu, Qian Luo, and Li Xin. 2016. "The four-chamber hydraulic cylinder." *2016 IEEE International Conference on Aircraft Utility Systems (AUS)*. IEEE.

Yang, Huayong, Bin Feng, and Guofang Gong. 2011. "Measurement of Effective Fluid Bulk Modulus in Hydraulic System." *Journal of Dynamic Systems, Measurement, and Control* 133 (6).